Efficient Planar Heterojunction Perovskite Solar Cells with Li-doped Compact TiO_2 Layer

Detao Liu[a], Shibin Li[a*], Peng Zhang[a], Yafei Wang[a], Rui Zhang[a], Hojjatollah Sarvari[b], Feng Wang[a,b], Jiang Wu[c], Zhiming Wang[d], and Zhi David Chen[a,b*]

[a] State Key Laboratory of Electronic Thin Films and Integrated Devices, and School of Optoelectronic Information, University of Electronic Science and Technology of China (UESTC), Chengdu, Sichuan 610054, China

[b] Department of Electrical & Computer Engineering, and Center for Nanoscale Science & Engineering, University of Kentucky, Lexington, Kentucky 40506, USA

[c] Department of Electronic and Electrical Engineering, University College London, Torrington Place, London WC1E 7JE,United Kingdom

[d] Institute of Fundamental and Frontier Sciences, University of Electronic Science and Technology of China, Chengdu, 610054, China

*Corresponding authors: shibinli@uestc.edu.cn, zhichen@engr.uky.edu

Abstract

Perovskite solar cells (PSCs) have been developed rapidly in recent time, and efficient planar PSCs are regarded as the most promising alternative to the Si solar cells. In this study, we demonstrated that Li-doping of compact TiO_2 can reduce the density of electron traps and increase the conductivity of the electron transport layer (ETL) of PSCs. Due to the improved electronic property of ETL, the Li-doped compact TiO_2 based planar heterojunction PSCs exhibit negligible hysteretic J-V behavior. Comparing with the undoped compact TiO_2 based PSCs, the power conversion efficiency (PCE) of the Li-doped compact TiO_2 film based PSCs is improved from 14.2% to 17.1%. Fabrication of highly efficient planar PSCs provides a pathway for commercialization of PSCs.

Keywords

Li-doping TiO_2; Planar heterojunction perovskite solar cells; Less- hysteresis; $CH_3NH_3PbI_3$.

Introduction

Sunlight is regarded as the most promising replacement for fossil fuels because it is a clean, cheap, abundant and renewable energy source. However, the cost of solar cells is still too high comparing to fossil fuels. To reduce the cost of the solar cells, scientists have developed the third-generation solar cells including organic solar cells, dye-sensitized solar cells, and perovskite solar cells (PSCs). Among the third-generation solar cells, the power conversion efficiency (PCE) of PSCs has increased rapidly. The PCE of PSCs has increased from 6.5 % to over 21.0 % from 2011 to 2016[1, 2]. The light absorber of the PSCs is $APbX_3$ ($A=CH_3NH_3$, $(NH_2)_2CH_2$ or Cs, X= I, Br or Cl) film. Because of their low cost and high efficiency, PSCs are considered as the most promising replacement of silicon solar cells.

The PSCs consist of a cathode, an electron transport layer (ETL), a light absorption layer, a hole transport layer (HTL) and an anode[3-5]. The ETL plays an important role in blocking holes and transporting electrons. Although there are many types of materials used for transporting electrons and blocking the holes, most of the state-of-the-art PSCs are based on TiO_2[2, 6-8]. There are two types of perovskite solar cells based on TiO_2, one is the planar hererojunction solar cells, and the other one is the mesoporous-structure solar cells. Up to now, the best PSC is the mesoporous-structure solar cell that contains a mesoporous TiO_2 layer[2, 6-8]. The mesoporous TiO_2 layer can collect electrons and achieve the balance between the hole flux and the electron flux effectively due to its larger surface area. Because of the balance between the hole flux and the electron flux, the mesoporous-structure PSCs have less hysteresis. However, the mobility of electrons in the TiO_2 is much lower than the mobility of electrons in the perovskite layer and the transport length of electrons in the

mesoporous layer is much longer than that in the compact TiO_2 layer[9]. Therefore, the conductivity of TiO_2 limits the improvement of the performance of PSCs. If extracting electrons at the interface between the perovskite layer and ETL in the planar-structure PSCs can be accelerated, high-performance planar PSCs may also be realized. Planar heterojunction PSCs also have a simple fabrication procedure, which is helpful for reducing cost. Effort has been made to improve the performance of the planar heterojunction PSCs[10-14]. Chen et al. employed the [6,6]-phenylC61-butyric acid methyl ester (60-PCBM) to modify the TiO_x surface and achieved a PCE of 17.6% with negligible hysteresis[12]. Konrad dramatically improved PCE and reduced hysteresis of PSCs by using an ultra-thin C60 layer to replace the TiO_2 layer[13]. Heetae Yoon also utilized the C60 layer as the ETL, and the PCE that extracted from both the reverse-scan I-V curve and the forward-scan I-V curve was over 19.11%[14]. A number of studies report that modification of the compact TiO_2 layer can enhance the performance of the planar heterojunction solar cells, but most of these methods used to modify the TiO_2 layer are complicated[15-18]. Developing an easier method to modify the compact TiO_2 is very important. It is reported that lithium (Li) can passivate the defects in the TiO_2 film, especially the defects on the surface, and increase the conductivity of TiO_2. Therefore, the Li-doped TiO_2 is beneficial to the performance of the mesoporous-structure PSCs, and especially the hysteresis of the I-V curves[19, 20]. However, there are no reports that focus on Li-doped compact TiO_2 (Li:TiO_2) layers in the planar heterojunction PSCs. It is yet to demonstrate whether the Li:TiO_2 can improve the performance of the planar solar cells or not and it is very meaningful to do so due to the commercial potential of planar heterojunction PSCs.

In this work, we developed Li-doped compact TiO_2 layers used as ETL in the planar heterojunction PSCs and achieved the best PCE of 17.1%. We studied how the Li doping affects the performance of the planar heterojunction PSCs using current-voltage characterization and Electronic Impedence Spectroscopy (EIS). We also studied the Li doping status in the compact TiO_2 layer using X-ray photospectroscopy (XPS). The PCE of our planar PSCs fabricated using Li-doped compact TiO_2 film as ETL increased from 14.2% to 17.1% with negligible hysteresis compared with the undoped one. The stable PCEs of the Li-doped PSCs obtained from the maximum power point are similar to those obtained from forward and reverse scan I-V curves.

Result and Discussion

To study the elemental composition of the Li-treated and untreated compact TiO_2 layers after sintering, XPS characterization was carried out. From Figure S1(a), we know that there are negligible traces of sulphur and fluorine from the LiTFSI precursor because LiTFSI was oxidized in air flow when heated to a high temperature. There is no obvious difference between Ti 2p spectra of the treated and untreated samples. All those results are consistent with Ref. [19]. The O1s spectra in Figure 1(a), 1(b) show that Li:TiO_2 exhibits a more pronounced shoulder at the higher binding energy side of the main peak compared with the undoped TiO_2. It is also the same as the results in Ref. [19]. The area ratio between the main peak and the shoulder peak of Li:TiO_2 and that of undoped TiO_2 are 3.48 and 5.14, respectively. According to the previous reports of other groups, the more pronounced shoulder at higher binding energy related to oxygen interaction with Lithium[19, 21]. We observed Ti 3s peaks in both Li:TiO_2 and TiO_2 (Figure S1) and it's same as the Ref. [20]. In

our experiments, the signal of Li in the XPS spectrum (Figure S1(b)) is weak, but distinct. The ratio of two peaks of O 1s suggests that Li was doped into the TiO_2 film. To investigate the effects of Li-doping on the electron trap density in the TiO_2 films, we measured the I-V curves of TiO_2 film with contacts, as shown in inset of Figure 1(c). The log-log plot of I-V curves in Figure 1(c) indicates that current increases linearly with voltage at the low bias voltage region. At the higher bias voltage region, current increases at a much higher slope. The transition point is the ohmic to trap filled limit transition point (V_{TFL}) and related to the trap density (N_t) linearly[20, 22]. The value of V_{TFL} increases as electron traps. From the I-V curves, we can estimate the values of V_{TFL}. The V_{TFL} of devices based on TiO_2 (1.39 V) is higher than that based on Li:TiO_2 (0.96 V). According to the relation between electron traps and V_{TFL}, the density of electron traps in the TiO_2 film is much higher than that in the Li:TiO_2 film. It is clear that Li-doping can passivate the electron traps.

We measured the optical absorption in the visible and UV light range (Figure 1(d)) to understand the optical properties. From the curves, we know that there is little absorption in the range of 350-800 nm and high absorption in the range of 300-350 nm due to the bandgap of TiO_2. The absorption curve of Li-doped TiO_2 almost overlaps that of undoped TiO_2. Therefore, it is concluded that the light absorption of TiO_2 is not affected by Li-doping.

The steady photoluminescence (PL) studies were conducted in an attempt to investigate the extracting rate of electrons that were generated by the light in the perovskite layer. The devices structure consists of the perovskite layer on the compact TiO_2 without a hole transport layer (HTL). From Figure 2(a), the steady PL intensity of the sample with Li-doping is lower than the one without Li-doping. It means that there is reduced charge recombination

in the perovskite layers which were deposited on the Li-treated TiO_2 layer. It is known that recombination of charges highly depends on the concentration of hole-electron pairs. Thus reduced charge recombination suggests less hole-electron pairs. In our case, it suggests lower concentration of the electrons in the perovsktie layer due to absence of HTL. Therefore, the ETL with Li-treating can extract electrons more effectively.

EIS was conducted to describe the charge transfer process and the Nyquest plot is shown in Figure 2(b). The Nyquist plot can be used to distinguish the charge transfer/ transport and the charge recombination at interfaces between different films [23-31]. The EIS was measured at a voltage bias of 0 V under one-sun light intensity in complete solar cells whose structures were shown in Figure 3(a) and Figure 3(b), respectively. The cross-sectional image of PSCLT clearly shows the complete solar cells consist of FTO layer, compact TiO_2 layer (~50nm), perovskite film (~350nm), Spiro-OMeTAD (~130nm) and gold layer (~110nm). The Nyquist plot exhibits that there are two arcs or semicircles. The first arc is related to the charge-transfer process at the counter electrode, the adjacent second arc is attributed to the recombination in the interface between different films[23, 31]. The plot was fitted with an equivalent circuit (the inset of Figure 2(b)) and resistances of the fitting results were shown in Table 1. The R_{tr} of the perovskite solar cells based on Li:TiO_2 (PSCLT) (54.80 Ω) is smaller than that of the perovskite solar cells based on conventional TiO_2 (PSCT) (79.64 Ω) due to the higher conductivity of Li:TiO_2. From the plot, the second arc of PSCLT is much larger than that of PSCT. The larger R_{rec}, related to the larger second arc in the plot, implies decreased recombination constant (K_{rec}) in the solar cells. It can be concluded that the recombination in PSCLT is much smaller than that in PSCT.

It is known that some oxygen atoms can easily move away from the TiO_2 lattice especially at the surface of the TiO_2 and thus there are some Ti elements with valency +4 (Ti^{4+}) that form dangling bonds, which were named as the oxygen vacancies[33, 34]. The dangling bonds easily trap electrons when the electrons transport in the TiO_2 layer. We propose the following hypothesis based on the above analysis and previous literatures that published by others[13,33]. Li-treating induces partial reduction of Ti^{4+} to Ti element with valency +3 (Ti^{3+}) within the TiO_2 lattice which was clarified in Ref. [23]. From the lower V_{TFL} of the Li:TiO_2, Ti^{3+} can passivate the electronic defects or trap states that originate from oxygen vacancies within the TiO_2 lattice, which was the same as the Al-doping in the TiO_2 layer[35]. How the Ti^{3+} elements come into being and passivate the electronic defects or trap states was shown in the Figure 2(c)-(f).

Figure 4(a) shows the current density - voltage (J-V) characteristic of the best performing planar PSCs with and without Li-doped compact TiO_2 layers. The device performance parameters which were extracted from the J-V curves in the Figure 4(a) were list in Table 2. From the curves and Table 2, we can see that both the open circuit voltage (V_{oc}) and the fill factor (FF) of PSCLT are higher than those of PSCT. V_{oc} of the PSCs increases from 1.01V to the 1.08V, suggesting less energy loss of electrons. FF increases from 59.45% to 68.02% due to reduction of the series resistance (R_s) and increase of the shunt resistance (R_{sh}). The decrease of R_s indicates higher mobility when electrons transports in the TiO_2 layer. The increase of the R_{sh} results from fast extraction of electrons and less trap-assisted recombination. Faster extraction of electrons results in less chances for electrons to recombine with holes. To make sure repeatability of the results, we fabricated more than 16

solar cells in each kind. The PCE and other related electrical parameters extracted from the I-V curves were shown in Figure 4(c)-(f). The dispersions of all parameters clearly manifest that PSCLT has remarkable improvement in the performance comparing with the control samples. The trap-assisted recombination of electrons in the TiO_2 layer is inhibited more effectively because of reduction of deep traps, which was beneficial to higher V_{oc} and FF. ETL is more conductive for electrons after Li-doping, resulting in more effective electron extraction and increase in short-circuit current density. To understand the reason for the increment of short-circuit current density, we also measured the EQE of both kinds of solar cells as shown in Figure 4(b). From the plot, it can be seen that the EQE of the PSCTs is much less than that of PSCLTs in the long wavelength range. The photons in the longer wavelength range have lower energy and electrons induced by photons also have lower energy. If the electron extraction capability of the ETL is weak, lower-energy electrons are more easily trapped before injecting into ETL[36]. The PL intensities of perovskite on ETLs with and without Li-doping suggests that electron extraction of Li:TiO_2 is stronger than that of TiO_2 due to the lower conduction band (Figure 3(c)).

The hysteresis of the PSCs is shown in Figure 5(a),(c). To compare two types of devices effectively, we chose the samples of which V_{OC} were similar. The PSCLT has a PCE of 16.21% in the reverse J-V curve and 16.17% in the forward J-V curve. From Figure 5(a), it can be seen that the I-V curves of the PSCLT with forward and reverse direction scans almost overlap each other, suggesting negligible hysteresis. The stable PCE that measured at the maximum power point is 16.69% (Figure 5b). It is very close to the PCE that is extracted from the J-V curve. But PSCT only has a PCE of 13.22% in the reverse-direction scan of the

J-V curve and 9.63% in its forward-direction scan. The hysteresis of the J-V curves is similar as the result of ref. [37]. The stable PCE of PSCT is 11.48% (Figure 5(d)), which is much lower than the PCE that is extracted from the reverse-direction scan of the J-V curve. The differences are mainly due to the FF difference, which can be reduced via doping the compact TiO_2 with Li. The mechanism for hysteresis of PSCs is still unclear. Some studies showed that the imbalance between the hole flux and the electron flux maybe one of the reasons for the hysteresis. Therefore, reduction of hysteresis in this work may be due to more efficient extraction of electrons that was identified by the stable PL so that the balance between the electron flux and the hole flux is achieved.

Conclusion

We studied the effectiveness of doping the compact TiO_2 with Li-element for planar perovskite solar cells. It is found that Li-doping of TiO_2 reduces the density of electron traps dramatically without negative effect on optical properties. Based on the stable PL, we found that electrons in the perovskite films can extracted more efficiently by Li:TiO_2 than conventional TiO_2. The FF was improved due to reduced R_s and increased R_{sh} after Li-doping of the compact TiO_2 layer. Reduction of R_s is due to higher mobility of Li:TiO_2 and more effective extraction of electrons, which also helps increase of J_{SC}. Larger R_{sh} originates from reduced recombination which is suggested by larger recombination resistance of the EIS. Larger R_{sh} also results in higher V_{OC}. The best PCE of planar solar cells has increased from 14.2 % to 17.1 % after Li-doping of the compact TiO_2 layer.

Acknowledgement

This work was supported by National Natural Science Foundation of China under Grant

Nos.61474016 and 61405026, 61371046, 61421002, 6157031208, 61471085, and National Higher-education Institution General Research and Development Fund (ZYGX2014J044), Projects of International Cooperation of Sichuan Province (No.2014HH0041). This work was also partially supported by University of Kentucky.

Supporting Information Available: Detailed description of XPS of the TiO_2 film and Li:TiO_2 film. The SEM, absorbance and XRD of the perovskite film.

Method

Solar cell fabrication: FTO glasses were cleaned using acetone, ethanol, and DI water in the ultrasonic bath for 15 min, respectively. A 50-nm-thick TiO_2 compact layer was then deposited on the substrates by spray pyrolysis at 500℃ using a commercial titanium diisopropoxide bis(acetylacetonate) solution (75% in 2-propanol, Sigma-Aldrich) diluted in ethanol (1:39, volume ratio) as precursor and oxygen as carrier gas. After cooling to room temperature (25℃), the substrates were treated in an 0.04 M aqueous solution of $TiCl_4$ for 30 min at 70℃, rinsed in DI water and dried at 500℃ for 30 min. For the Li-doping solar cells, 0.1M Li-TFSI solution was spin-coated on substrates and then the substrates were annealed at 500℃ for 30min. The perovskite films were deposited by spin coating onto the Li-doped TiO_2 substrates. For the reference solar cells, the perovskite films were deposited by spin coating onto the TiO_2 substrates without treatment. The deposition method of perovskite was same as that in Ref. [8,37]. After perovskite was deposited, the spiro-OMeTAD solution used as the hole transport layer (HTL) was spin coated on the substrates. The spiro-OMeTAD solution was prepared by dissolving 72.3 mg (2,29,7,79-tetrakis(N,N-di-p-methoxyphenylamine)-9,9-spirobifluorene) (spiro-MeOTAD), 28.8 ml 4-tert-butylpyridine, 17.5 ml of a stock solution of 520 mg ml21 lithium bis(trifluoromethylsulphonyl)imide in acetonitrile and 29 ml of a solution of 300mg/ml tris(2-(1H-pyrazol-1-yl)-4-tert-butylpyridine)-cobalt(III) bis(trifluoromethylsulphonyl)imide in acetonitrile in 1 ml chlorobenzene. Finally, 100nm of Au top electrode was thermally evaporated onto the HTL.

Device Characterization:

The current–voltage characteristics of solar cells were measured using Keithley Model 2400 source measuring unit under solar-simulated light (Newport Oriel Solar 3A Class AAA, 64023A). The AM 1.5G sun light (100 mW/cm^2) was calibrated using a standard Si-solar cell (Oriel, VLSI standards). The EIS measurements were performed using electrochemical workstation (chi660d). The applied voltage perturbation had an AC amplitude of 35 mV (rms) with a frequency from 1 MHz to 100 Hz. The impedance parameters were simulated by fitting of the impedance spectra using Zview software. The stable PL was characterized using F-4600. The UV-vis light absorption was measured using ultraviolet-visible (UV–vis) spectrophotometer (Schimadzu UV-3101 PC). XPS was measured using the Kratos XSAM 800 X-Ray Photoelectron Spectrometer.

Reference

[1] J.H. Im, C.R. Lee, J.W. Lee, S.W. Park, N.G. Park, Nanoscale 3 (2011) 4088-4093.

[2] M. Saliba, T. Matsui, J.-Y. Seo, K. Domanski, J.-P. Correa-Baena, M.K. Nazeeruddin, S.M. Zakeeruddin, W. Tress, A. Abate, A. Hagfeldt, M. Grätzel, Energy Environ. Sci. 9 (2016) 1989-1997.

[3] M.A. Green, A. Ho-Baillie, H.J. Snaith, Nat. Photonics 8 (2014) 506-514.

[4] Y. Wang, S. Li, P. Zhang, D. Liu, X. Gu, H. Sarvari, Z. Ye, J. Wu, Z.M. Wang, Z.D. Chen, Nanoscale, (2016) DOI: 10.1039/C6NR07076K.

[5] T.C. Sum, N. Mathews, Energy Environ. Sci. 7 (2014) 2518-2534.

[6] W.S. Yang, J.H. Noh, N.J. Jeon, Y.C. Kim, S. Ryu, J. Seo, S.I. Seok, Science 348 (2015) 1234-1237.

[7] D. Bi, W. Tress, M.I. Dar, P. Gao, J. Luo, C. Renevier, K. Schenk, A. Abate, F. Giordano, J.P. Correa Baena, J.D. Decoppet, S.M. Zakeeruddin, M.K. Nazeeruddin, M. Gratzel, A. Hagfeldt, Sci. Adv. 2 (2016) e1501170.

[8] N. Ahn, D.Y. Son, I.H. Jang, S.M. Kang, M. Choi, N.G. Park, J. Am. Chem. Soc. 137 (2015) 8696-8699.

[9] J.H. Heo, H.J. Han, D. Kim, T.K. Ahn, S.H. Im, Energy Environ. Sci. 8 (2015) 1602-1608.

[10] F. Huang, Y. Dkhissi, W. Huang, M. Xiao, I. Benesperi, S. Rubanov, Y. Zhu, X. Lin, L.

Jiang, Y. Zhou, A. Gray-Weale, J. Etheridge, C.R. McNeill, R.A. Caruso, U. Bach, L. Spiccia, Y.-B. Cheng, Nano Energy 10 (2014) 10-18.

[11] H. Huang, J. Shi, L. Zhu, D. Li, Y. Luo, Q. Meng, Nano Energy 27 (2016) 352-358.

[12] C. Tao, S. Neutzner, L. Colella, S. Marras, A.R. Srimath Kandada, M. Gandini, M.D. Bastiani, G. Pace, L. Manna, M. Caironi, C. Bertarelli, A. Petrozza, Energy Environ. Sci. 8 (2015) 2365-2370.

[13] K. Wojciechowski, T. Leijtens, S. Siprova, C. Schlueter, M.T. Horantner, J.T. Wang, C.Z. Li, A.K. Jen, T.L. Lee, H.J. Snaith, J. Phys. Chem. Lett. 6 (2015) 2399-2405.

[14] H. Yoon, S.M. Kang, J.-K. Lee, M. Choi, Energy Environ. Sci. (2016) DOI:10.1039/c6ee01037g.

[15] M.C. Wu, S.H. Chan, M.H. Jao, W.F. Su, Solar Energy Materials and Solar Cells, 157 (2016) 447-453.

[16] Y. Li, J.K. Cooper, W. Liu, C.M. Sutter-Fella, M. Amani, J.W. Beeman, A. Javey, J.W. Ager, Y. Liu, F.M. Toma, I.D. Sharp, Nat. Commun. 7 (2016) 12446.

[17] X. Yin, Y. Guo, Z. Xue, P. Xu, M. He, B. Liu, Nano Research 8 (2015) 1997-2003.

[18] H. Zhou, Q. Chen, G. Li, S. Luo, T.B. Song, H.S. Duan, Z. Hong, J. You, Y. Liu, Y. Yang, Science 345 (2014) 542-546.

[19] F. Giordano, A. Abate, J.P. Correa Baena, M. Saliba, T. Matsui, S.H. Im, S.M. Zakeeruddin, M.K. Nazeeruddin, A. Hagfeldt, M. Graetzel, Nat. Commun. 7 (2016) 10379.

[20] J.H. Heo, M.S. You, M.H. Chang, W. Yin, T.K. Ahn, S.-J. Lee, S.-J. Sung, D.H. Kim, S.H. Im, Nano Energy 15 (2015) 530-539.

[21] S. Södergren, H. Siegbahn, H. Rensmo, H. Lindström, A. Hagfeldt, S.-E. Lindquist, J. Phys. Chem. B 101 (1997) 3087-3090.

[22] D. Yang, R. Yang, X. Ren, X. Zhu, Z. Yang, C. Li, S.F. Liu, Adv. Mater. (2016) DOI: 10.1002/adma.201600446.

[23] H.S. Kim, J.W. Lee, N. Yantara, P.P. Boix, S.A. Kulkarni, S. Mhaisalkar, M. Gratzel, N.G. Park, Nano Lett. 13 (2013) 2412-2417.

[24] X. Dong, X. Fang, M. Lv, B. Lin, S. Zhang, J. Ding, N. Yuan, J. Mater. Chem. A 3 (2015) 5360-5367.

[25] D. Liu, J. Yang, T.L. Kelly, J. Am. Chem. Soc. 136 (2014) 17116-17122.

[26] S. Lee da, W. Kim, B.G. Cha, J. Kwon, S.J. Kim, M. Kim, J. Kim, D.H. Wang, J.H. Park, ACS Appl. Mater. Inter. 8 (2016) 449-454.

[27] B.J. Kim, D.H. Kim, Y.-Y. Lee, H.-W. Shin, G.S. Han, J.S. Hong, K. Mahmood, T.K. Ahn, Y.-C. Joo, K.S. Hong, N.-G. Park, S. Lee, H.S. Jung, Energy Environ. Sci. 8 (2015) 916-921.

[28] D. Yang, R. Yang, J. Zhang, Z. Yang, S. Liu, C. Li, Energy Environ. Sci. 8 (2015) 3208-3214.

[29] S. Wang, W. Yuan, Y.S. Meng, ACS Appl. Mater. Inter. 7 (2015) 24791-24798.

[30] W. Sun, Y. Li, S. Ye, H. Rao, W. Yan, H. Peng, Y. Li, Z. Liu, S. Wang, Z. Chen, L. Xiao, Z. Bian, C. Huang, Nanoscale (2016) DOI: 10.1039/c6nr01927g.

[31] A. Dualeh, T. Moehl, N. Tetreault, J. Teuscher, P. Gao, M.K. Nazeeruddin, M. Gratzel, ACS nano 8 (2014) 362-373.

[32] G. Veerappan, D.W. Jung, J. Kwon, J.M. Choi, N. Heo, G.R. Yi, J.H. Park, Langmuir 30 (2014) 3010-3018.

[33] T. Leijtens, G.E. Eperon, S. Pathak, A. Abate, M.M. Lee, H.J. Snaith, Nat. Commun. 4 (2013) 2885.

[34] C. Di Valentin, G. Pacchioni, A. Selloni, J. Phys. Chem. C 113 (2009) 20543-20552.

[35] S.K. Pathak, A. Abate, P. Ruckdeschel, B. Roose, K.C. Godel, Y. Vaynzof, A. Santhala, S.I. Watanabe, D.J. Hollman, N. Noel, A. Sepe, U. Wiesner, R. Friend, H.J. Snaith, U. Steiner, Adv. Funct. Mater. 24 (2014) 6046-6055.

[36] A. Agresti, S. Pescetelli, L. Cinà, D. Konios, G. Kakavelakis, E. Kymakis, A.D. Carlo, Adv. Funct. Mater. 26 (2016) 2686-2694.

[37] H.S. Kim, I.H. Jang, N. Ahn, M. Choi, A. Guerrero, J. Bisquert, N.G. Park, J. Phys. Chem. Lett. 6 (2015) 4633-4639.

Figure 1. (a) The XPS peaks of the O1s in the Li:TiO_2 film,(b) The XPS peaks of the O1s in the conventional TiO_2 film, (c) I-V curves for the FTO/TiO_2 or Li:TiO_2/Au and (d) absorption of the Li:TiO_2 and TiO_2.

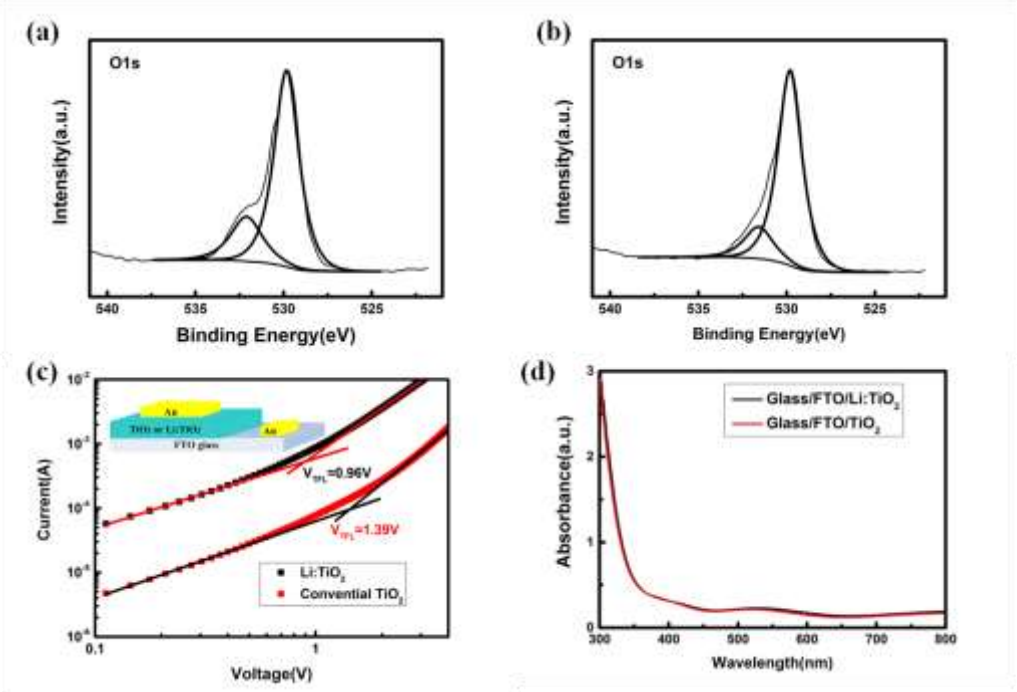

Figure 2. (a) Stable PL curves of perovskite films on Li-treated TiO_2 and conventional TiO_2, (b) EIS Nyquist plots of the perovskite solar cells based on Li:TiO_2 and TiO_2, (c) oxygen vacancies in TiO_2 lattice before passivation，(d) electronic traps blow the conduction band in TiO_2, (e) the Ti^{3+} that exist in TiO_2 lattice after the Li-treating and (f) the energy diagram after traps have been passivated.

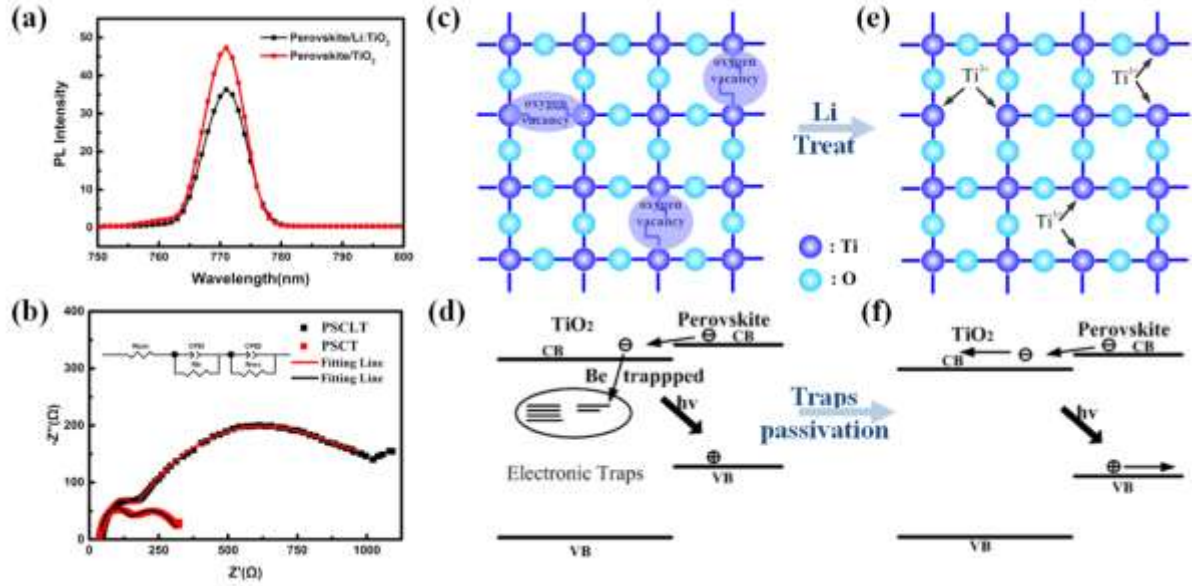

Figure 3. (a) Cross-sectional SEM images of PSCLT, (b) Schematic illustration of the device structure of a planar heterojunction $MAPbI_3$ hybrid solar cell and (c) energy band diagram of PSCs.

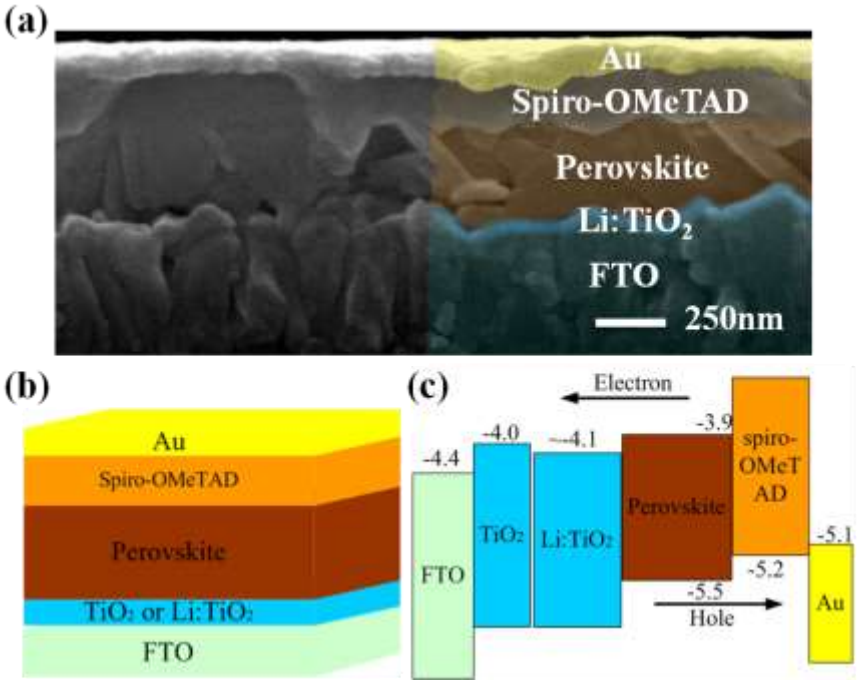

Figure 4. (a) The reverse-direction-scan J-V curves of the best-performance PSCs based on Li-treated TiO_2 and conventional TiO_2, (b) EQE curves and integrated current density of different samples, (c)~(f) the V_{OC}, FF, J_{SC}, PCE versus two kinds of solar cells.

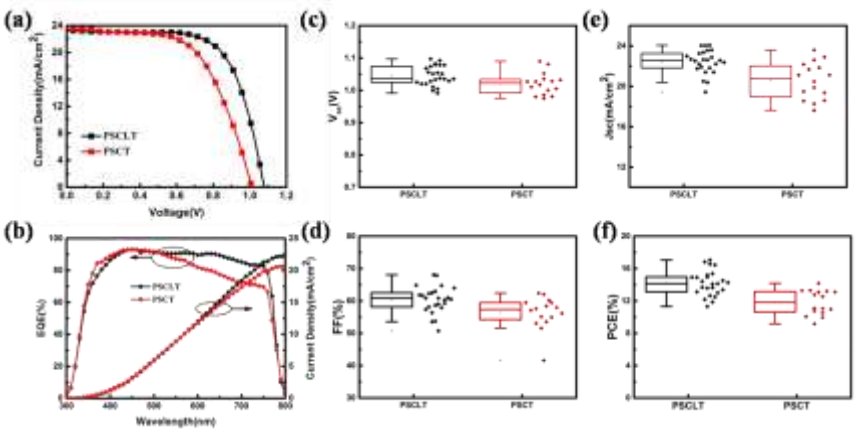

Figure 5. (a) the J-V curves of the forward and reverse direction scans for the PSC based on Li:TiO_2, (b) the stable output current density and PCE at the max power point (0.8V) of the Li-doping sample, (c) the J-V curves of the forward and reverse direction scans for the PSC based on conventional TiO_2, (d) the stable output current density and PCE at the max power point (0.71V) of the reference sample.

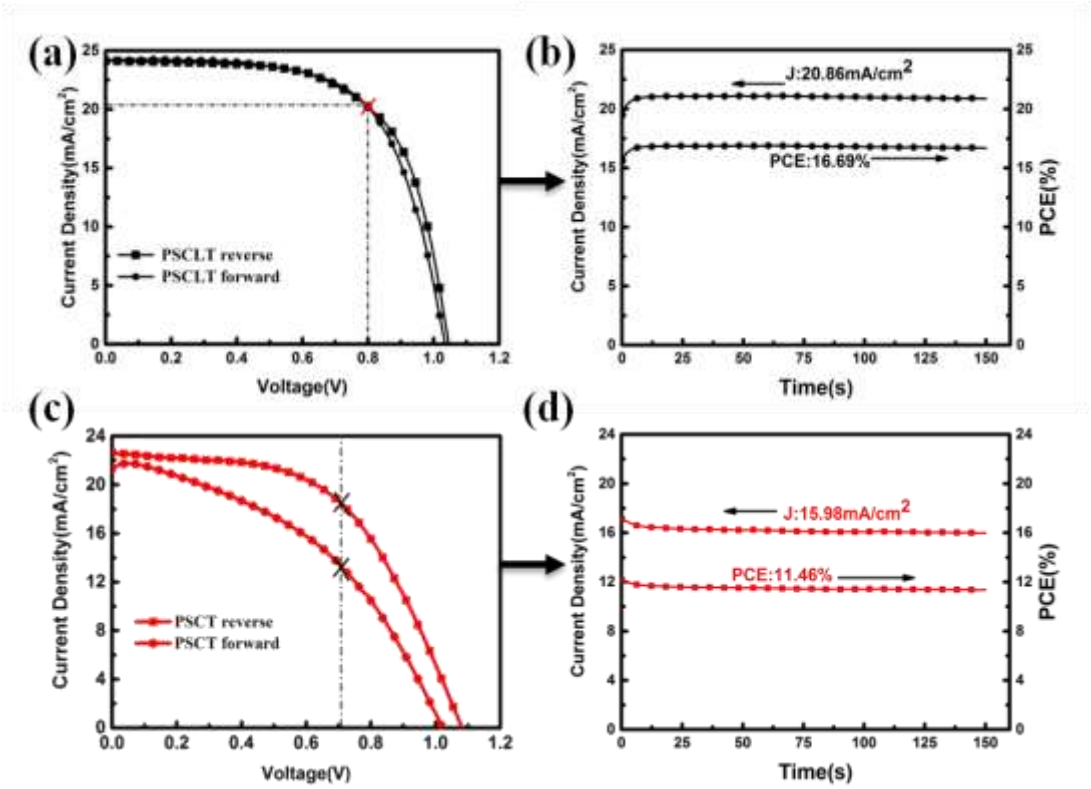

Table 1 Fitting results of the Nyquist plot

	R_{con}(Ω)	R_{tr}(Ω)	R_{rec}(Ω)
PSCLT	44.39	54.80	961.1
PSCT	40.9	79.64	216.8

Table 2 Performance parameters of the best devices

	V_{OC}(V)	J_{SC}(mA/cm^2)	FF(%)	PCE(%)	R_s(Ω•cm^2)	R_{sh}(Ω•cm^2)
PSCLT	1.08	23.26	68.02	17.06	7.46	1205.45
PSCT	1.01	23.59	59.47	14.18	9.81	503.60

V_{OC}: open-circuit voltage, J_{SC}: short-circuit current density, FF: fill factor, PCE: power conversion efficiency, R_s: series resistance, R_{sh}: shunt resistance.